Performance and Reliability Optimization for Aerospace Systems subject to Uncertainty and Degradation

David W. Miller, Scott A. Uebelhart and Carl Blaurock

MIT Space Systems Laboratory

Final Report
March 26, 2004

This research was supported by NASA's Langley Research Center, contract #NAG1-01025, with Sean Kenny as Technical Monitor and Sharon Leah Brown as MIT Fiscal Officer.

Contents

1 Introduction

1.1 Objective

This report summarizes work performed by the Space Systems Laboratory (SSL) for NASA Langley Research Center in the field of performance optimization for systems subject to uncertainty. The objective of the research is to develop design methods and tools to the aerospace vehicle design process which take into account lifecycle uncertainties. It recognizes that uncertainty between the predictions of integrated models and data collected from the system in its operational environment is unavoidable. Given the presence of uncertainty, the goal of this work is to develop means of identifying critical sources of uncertainty, and to combine these with the analytical tools used with integrated modeling. In this manner, system uncertainty analysis becomes part of the design process, and can motivate redesign. The specific program objectives were:

1. To incorporate uncertainty modeling, propagation and analysis into the integrated (controls, structures, payloads, disturbances, etc.) design process to derive the error bars associated with performance predictions.

2. To apply modern optimization tools to guide in the expenditure of funds in a way that most cost-effectively improves the lifecycle productivity of the system by enhancing the sub-system reliability and redundancy.

The results from the second program objective are described in [21]. This report describes the work and results for the first objective: uncertainty modeling, propagation, and synthesis with integrated modeling.

1.2 Report Overview

This report is broken into four parts, covering the areas researched. Section 2 provides background on uncertainty in system design as investigated in the SSL. It includes a literature search performed on propagation of uncertainty, and describes possible approaches to dealing with uncertain system interfaces. Section 3 uses knowledge on the sources of uncertainty along with data taken from the Multi-body Active Control Experiment (MACE) to experimentally derive uncertainty bounds for several parameters. Section 4 describes the change-of-variables propagation routine developed by SSL. Finally Section 5 integrates all of the research together and shows an example problem of how to use uncertainty analysis in the design process.

This integration is performed in the DOCS analysis environment. DOCS (Disturbance-Optics-Controls-Structures toolbox), developed at MIT and commercialized by Midé Technology Corporation is a MATLAB® toolbox developed for the creation and dynamical analysis of integrated models (figure 1). Integrated aerospace models can be created using finite element program, control systems, and disturbance or optics models. These models are first numerically conditioned, and then can be run through a host of suites. These include predicting the root-mean-square (RMS) values of performance metrics, sensitivity analyses which can be coupled with gradient-based optimization, and uncertainty analysis to include error bars with the predicted performance values. The research described by this

report has used and built upon DOCS; specifically the boxes "Uncertainty Database" and "Uncertainty Analysis" in figure 1 were advanced.

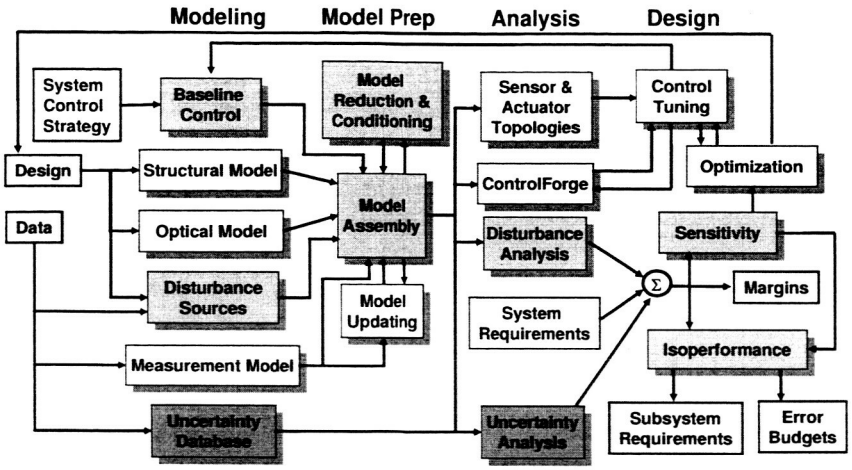

Figure 1: Roadmap for the DOCS framework. Red boxes indicate that new capabilities have been added.

1.3 MACE

The Multi-body Active Control Experiment (MACE) is an example of an aerospace system to illustrate the use of uncertainty in design. MACE (figure 2) is a 1.6 meter long flexible structure designed and built in cooperation by MIT, Payload Systems Incorporated, Lockheed Martin Missiles and Space Company, and NASA Langley Research Center. It was originally built to investigate high precision pointing and vibration control of flexible structures [19], and has been used in developing techniques for system identification, model updating, and nonlinear control.

MACE consists of four struts connected axially to each other, with aluminum nodes at each interface. Three of the struts are polycarbonate, and the fourth is an active strut with piezoelectric actuators. At the center of this boom is a reaction wheel assembly consisting of three momentum wheels. At each end are gimbals in the X- and Z-directions, which provide disturbance inputs on one side, and control actuation on the other. Below the gimbals are 0.7 meter long flexible appendages.

MACE comes fully instrumented with a complete actuator/sensor package. There 20 sensors comprised of rate gyros, optical encoders, strain gages and reaction wheel tachometers. The 9 actuators are made up of gimbals, three reaction wheels, and piezo-electric active struts. A separate Electronics Support Module (ESM) provides real time control, and any necessary actuator and sensor conditioning.

Figure 2: Illustration of the MACE testbed.

2 Uncertainty in Systems Design

The challenge in validating high performance systems is that modeled performance predictions cannot be independently validated by systems level tests until they are in their operational environment, at which point it may be extremely difficult and costly to make gross changes to the design.

An alternative to systems testing is to validate the design using modeling, analysis, and lower-level testing. An illustration of this approach is shown in Figure 3. Since uncertainty will continue to exist in all models, its presence must also be taken into consideration. As yet, uncertainty in system design is not treated in a rigorous fashion. Nominal values of model results are tracked, but results are frequently given without any confidence intervals. Uncertainty safety factors are often used in place of any real knowledge of the system uncertainties. This highlights a need in current design practices to include uncertainty in the design process.

The goal of this research is to build a framework for uncertainty management in the design process for high performance systems. The research includes identifying model uncertainties, evaluating uncertainties to determine how much they affect the system performance, and tracking both sources of uncertainty, or inputs to the model, and overall system uncertainty, or model outputs, through the process. An overview of literature in the subject follows.

2.1 Literature Overview

There is a wealth of literature on the subject of uncertainty. Many papers have been written which use simple methods to place tolerance bounds about the nominal value for some metric. Researchers in such diverse fields as engineering, economics, and political science have applied uncertainty analysis techniques to models of everything from aerospace structures, bridges, and chemical processes, to economic trends and socio-environmental consequences [8]. All of these works tend to use one of a small handful of uncertainty techniques.

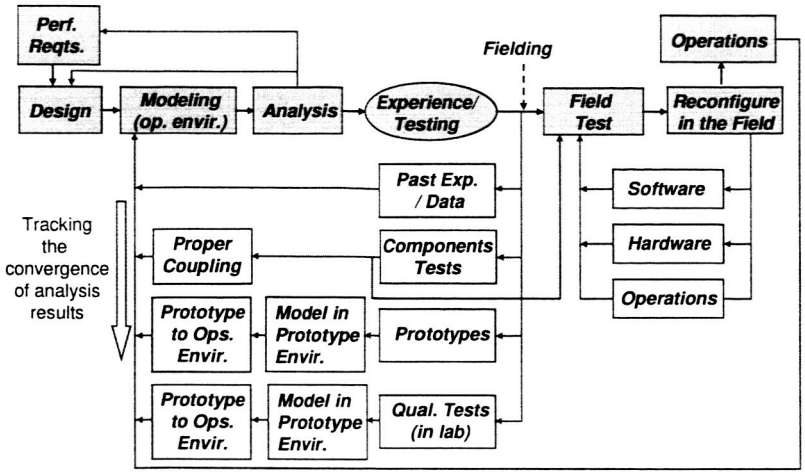

Figure 3: Design lifecycle paradigm, as developed at the MIT Space Systems Laboratory.

Below is a brief overview of the techniques, along with advantages and disadvantages.

The great majority of uncertainty analyses in literature deal with the propagation of an uncertain input (or inputs) through a model in order to determine the uncertainty of an output. These individual model propagation techniques can be grouped into bounded or probabilistic uncertainty descriptions, depending on whether the uncertainty on the input is described using lower and upper bounds, or by a probability density function. The propagation approaches will be described first, followed by a brief overview of related topics, and finally a look at those techniques dealing with uncertainty amongst several models.

2.1.1 Bounded Propagation Methods

Bounded uncertainty techniques place lower and upper bounds on the model output (figure 4). Gutierrez [11] describes several approaches. The first is the worst-case corners approach, in which the model is run at the lower and upper bound of each input parameter. Consider figure 5, where two parameters lead to four worst-case evaluations of the model. This is a relatively simple analysis with few parameters, though additional parameters quickly increase the computational burden.

The first-order sensitivity approach in [11] uses sensitivity information between the output performances σ and input parameters p to compute the performance bound based on small changes in p.

$$\Delta\sigma \approx \frac{\partial\sigma}{\partial p}\Delta p \tag{1}$$

Once the sensitivities are computed, the performance uncertainty $\Delta\sigma$ at different levels of Δp can be determined. Since this approach relies on first order gradient information, its validity is only as good as that of the gradient. Often this limits the approach to small perturbations in p.

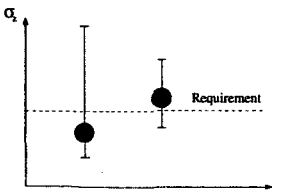

Figure 4: Uncertainty bounds provide a more complete picture than the nominal results alone; the left value nominally meets requirement, but with much greater uncertainty than the right value.

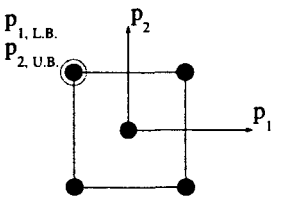

Figure 5: Example of worst-case bounds, where a point is selected at the lower bound (L.B.) and upper bound (U.B.) of each parameter.

Other techniques such as the Robust Control approach [11] and Linear Fractional Transformation [1] similarly produce a bounded uncertainty model. The key disadvantage of all of these approaches is that the bounds provide no information on the likelihood that a performance will be located at an extreme value. This makes it possible to reject a design that has an acceptably low but non-zero probability of failing to meet requirements.

2.1.2 Probabilistic Propagation Methods

A probabilistic uncertainty approach finds the probability density function (PDF) for model outputs, given the input PDFs. The uncertainty of an output can be described using standard probabilistic concepts such as mean and standard deviation. Instead of looking to see whether an upper bound exceeds performance requirement, the designer can report the probability that a design meets requirements.

Monte Carlo sampling is perhaps the best-known propagation technique, in which random samples based on the input PDF are run through the model. Once enough output data points have been collected, their mean and moments can be taken to form the output PDF. Reference [10] provides a good overview of Monte Carlo sampling, along with other sampling techniques that try to reduce the large computational time. These include Stratified Monte Carlo sampling, Quasi-Monte Carlo sampling, and Latin Hypercube sampling.

Melchers [18] describes the First- and Second-Order Reliability Methods (FORM and SORM), which determine the probability of failure of a system with normal random variable inputs. The limit state function, which defines the failure regions of the response, are approximated by either first or second order functions. Non-normal variables can be transformed to normal for approximate results.

Linear Covariance Propagation (LCP) assumes that Higher Order Terms (H.O.T.) in

the design objective function are negligible:

$$J(\alpha) = J_o + \frac{\partial J}{\partial \alpha} + H.O.T. \approx J_o + \frac{\partial J}{\partial \alpha} \tag{2}$$

where α is a vector of uncertain parameters. Under the assumption that α is a normally distributed vector random variable, $\alpha \sim N(\mu_\alpha, \Sigma_{\alpha\alpha})$, the variance of the objective can be computed from the sensitivity,

$$E[J] \approx J(\mu_\alpha) \tag{3}$$

$$E[J^2] \approx \frac{\partial J}{\partial \alpha} \Sigma_{\alpha\alpha} \frac{\partial J^T}{\partial \alpha} \tag{4}$$

When the parameters are independent, the contribution of each parameter to the variance of the output can be computed:

$$E[J^2] \approx \sum_{i=1}^{n_p} \frac{\partial J}{\partial \alpha_i} \sigma_{\alpha_i}^2 \frac{\partial J^T}{\partial \alpha_i} \tag{5}$$

where n_p is the number of parameters. An example of linear covariance propagation in shown in Section 5.

The change-of-variables routine involves the analytic PDF transformation [5] to propagate an input PDF through the model, producing an exact output PDF. This approach has been advanced in this research, and more information is provided in Section 4.

Disadvantages of probabilistic uncertainty techniques include the computational time required for these approaches, especially for very large models. The other key problem is the accuracy of input distributions. While the Gaussian distributions is often chosen because of its simplicity, it may not be the appropriate distribution for a given input. Distributions are also difficult to determine empirically because of the large number of tests required for confidence in the distribution. Testing hardware in which only a limited number of copies are available may not be statistically sound.

2.1.3 Related Fields

There are several areas related to uncertainty analysis that also bear consideration. Robust Design [16], including the contributions of Taguchi, is a large field, concerned with methods of design and manufacturing to reduce defects. Stochastic Finite Elements [9] include stochasticity in the finite element formulation itself, although doesn't appear to be as widely used as traditional finite element approaches coupled with uncertainty propagation tools.

Design of Experiments (DOE) [20] is a field in statistics that deals with how to set-up, run, and analyze experiments involving random phenomenon. It is a well developed field, but rarely is included in any discussion of engineering uncertainty. Although originally developed for agricultural and biological testing, it has been brought into the realm of deterministic computational simulation to help examine stochastic behavior [10]. Computer-based sampling procedures such as Latin Hypercube Sampling are examples of modern DOE, where the goal is to gain the maximum information from a limited number of runs of a simulation. The high computational cost of running many of the integrated modelling simulations motivates further study of this field for uncertainty analysis.

2.1.4 Uncertainties between Models

Most papers discussing uncertainty use one of the previous methods to consider the propagation of uncertainty through a single model. During a design lifecycle, many different models are used. New models are built with increasing complexity; data from testbeds are compared to models of the testbeds, and system components can be tested once available. As the models change, and as data becomes available, it becomes possible to map uncertainty across models and between similar structures. These require different tools than those used to propagate uncertainty through a single model. This branch of uncertainty analysis is much smaller, but several sources are available.

Maghami [17] and Lim [15] have considered uncertainty between substructure models connected by component mode synthesis. They consider not only the propagation of uncertainty from one substructure to the next, but also the effect that the substructure assembly process has on the dynamics of the entire system. This is elaborated upon in the next section.

Hasselman's [12] database of aerospace structures is a compilation of knowledge gained from previous flexible structures for estimating the uncertainty of new models. The differences between model and data from the historical structures are combined in covariance matrices. These covariances can then be used in a linear covariance propagation routine to estimate the similar differences in any new model of a similar structure. Bounds on the transfer functions of the new models are produced. This approach was used by the SSL to examine model uncertainty for the Space Interferometry Mission [4]. The method does lack from the limited number of historical structures in the database.

Campbell [6] describes uncertainty mapping between different configuration of a model. Using MACE as his example, he tests the structure on the ground and compares the results with the 1-g model. The differences are then mapped to the 0-g model in order to estimate the uncertainties of MACE as tested in the Space Shuttle.

These three examples of using uncertainties between or across models are rarities in the literature. Most often only the single step of propagating uncertainty through a single model is shown. Any greater attempt at uncertainty management through the design process is performed on an ad-hoc basis. A common industrial approach, for which very few literature references have been found, is to use Model Uncertainty Factors (MUFs). These are little more than factors of safety about the nominal output. (See reference [2] for an example on determining this factor for dynamic modes.)

2.2 Uncertainty Between Multiple Components

Consideration was given on how to account for uncertainty between system components modeled separately. A quick description of methods to examine single component uncertainty is given first, followed by an overview of component mode synthesis to combine component models. Lastly these ideas are synthesized into a framework that could analysis the role of uncertainty between model.

2.2.1 Single Component Uncertainty

Consider two components (figure 6). The dynamic response of each body, individually, is the time history $y(t)$ given some forcing function $F(t)$, which could be an impulse or entire time history. The response could be solved by integrating the dynamic equations of motion

$$\begin{aligned} M_i\ddot{x}_i(t) + C_i\dot{x}_i(t) + K_i x_i(t) &= \beta_i F(t) \\ y_i(t) &= C_{y_i} x_i(t) \end{aligned}$$

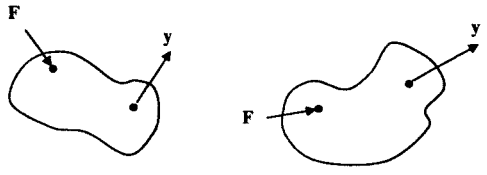

Figure 6: Generic uncertain components with transfer functions from inputs F to outputs y

for each body, i. The resulting dynamic response will be affected by any uncertainty in each model, either parametric in the M, C, or K matrices, or non-parametric in, for example, mismodeled elements or FEM fidelity errors. The input $F(t)$ is often stochastic in nature; as a disturbance input it is usually modeled as unity white noise fed through disturbance shaping filters. Therefore, the standard measure of dynamic response is the root-mean squared value of the output. This can be found directly from the time histories by taking the expectation of the square of the output values.

$$\sigma_y = \sqrt{E[y(t)^2]}$$

Instead of performing the integration, the RMS value can be found using the tools described in Gutierrez [11]. The easiest, perhaps, is the Lyapunov technique, for which the system must be described in state-space format

$$\begin{aligned} \dot{x} &= Ax + Bd \\ y &= Cx \end{aligned}$$

where the input d is unity white noise, and the state vector x includes states from an appended white-noise shaping filter. Note that the i subscripts denoting the individual components have been dropped for convenience. The root mean square value of the dynamic response is found by solving for the state covariance matrix Σ

$$A\Sigma + \Sigma A^T + BB^T = 0$$

and plugging it into

$$\sigma_y = \sqrt{C\Sigma C^T}$$

A simple and direct method for determining the uncertainty of this value is to using random sampling (Monte Carlo). A sample is chosen randomly from a set of inputs with given probability densities, and after running a sufficient number of cases the statistics of the outputs translate into the PDF of the output system. The major drawback of this approach is the large number of test runs required to adequately cover the sample space.

A more efficient method would be to use Latin Hypercube Sampling[10]. Each input probability density curve is subdivided into p regions of equal probability. If there are n uncertain parameters, then there exist p^n bins. One approach, termed Stratified Monte Carlo sampling, would sample from each and every bin once. The actual location a point is taken from a bin could be a set point, such as the probabilistic center of that bin, or could be randomly placed. Stratified Monte Carlo sampling could still require a large number of runs, so to speed the process even further Latin Hypercube Sampling takes only one sample from each region of each input, and thus requires a total of only p samples. Figure 7 shows a graphical description of this. The results can be similarly analyzed to produce PDFs or CDFs of the uncertain output.

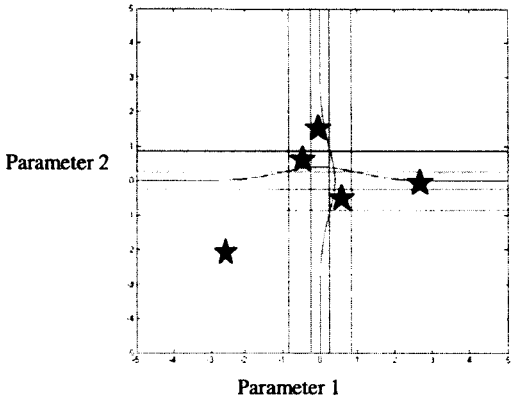

Figure 7: Illustration of Latin Hypercube Sampling

2.2.2 Transfer Functions of Joined Components

Either because different components are being build by different organization, or as a way to reduce the complexity of the global model, individual components are often modeled separately. In analyzing the system model, it is then often necessary to combine the component models in such a way that transfer functions $G(s) = Y(s)/F(s)$ can be constructed where the input F is on one component, and the output y is on the other.

There are several methods commonly used to assembly component models into a global system model. Blaurock [3] uses an acceleration feedback method, which inverts the interface inputs and outputs for one of the components, and treats the acceleration outputs from

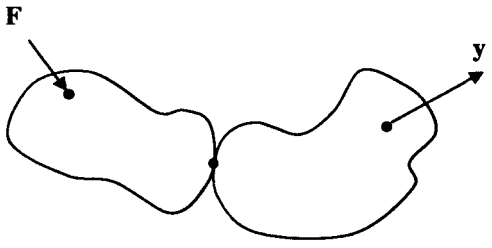

Figure 8: Two structures joined

the first model as force inputs to the second, and vice versa. Another popular method is Component Mode Synthesis [7]. This method will be described further.

Component mode synthesis finds a basis of Ritz vectors to span the space of the interior and boundary (or interface) degrees of freedom for each component. The individual component states are transformed with these component modes matrices, and the transformed models combined by enforcing that boundary degrees of freedom are constrained to each other.

The most popular variant of Component Model Synthesis is the Craig-Bampton method, first proposed by Craig and Bampton [13] with further elaboration in [14]. It obtains the transformation matrices by computing normal modes of the component interior points with the boundary degrees of freedom fixed. Constraint modes are found by setting each boundary degree of freedom to unity displacement or rotation, with no forces on the interior points. In the original papers the end goal of the analysis was to find modeshapes and frequencies of the unforced global system. Lim [15] considered substructure assembly from a controls sense, where inputs and outputs can be framed in a state-space manner. This was expanded upon in [17], where he also described uncertainties in the final synthesized models. These papers provide an excellent overview of the approach taken to find the assembled transfer functions. In addition the literature contains many other instances of component mode synthesis in use.

A derivation of the input/output transfer function follows. It starts with the component models A and B in a generic form.

$$\begin{aligned} M_A\ddot{x}_A + K_A x_A &= \beta_A F & \qquad M_B\ddot{x}_B x_B &= \beta_B F \\ y_A &= C_{yA}x_a & \qquad y_B &= C_{yB}x_B \end{aligned}$$

or, generally for any component i:

$$\begin{aligned} M_i\ddot{x}_i + K_i x_I &= \beta_i F \\ y_i &= C_{yi}x_i \end{aligned}$$

Next, identify those degrees of freedom (DOFs) that will be attached to the other component. Separate the states into those at the boundary j and those in the interior i.

$$x = \left\{ \begin{array}{c} x_i \\ x_j \end{array} \right\}$$

then the main state equation matrices can be divided as shown:

$$\begin{bmatrix} M_{ii} & M_{ij} \\ M_{ji} & M_{jj} \end{bmatrix} \begin{Bmatrix} \ddot{x}_i \\ \ddot{x}_j \end{Bmatrix} + \begin{bmatrix} K_{ii} & K_{ij} \\ K_{ji} & K_{jj} \end{bmatrix} \begin{Bmatrix} x_i \\ x_j \end{Bmatrix} = \begin{bmatrix} \hat{\beta} \\ 0 \end{bmatrix} F$$

Next write the physical coordinates in term of a Ritz approximation:

$$x_i = \Psi_i p_i$$

where x are the physical coordinates, p are the generalized coordinates, and Ψ are the pre-selected component modes. Methods of finding these Ritz vectors are described more fully in the literature on the subject, but generally use a combination of normal modes of each of the components, combined with a basis of constraint modes at the component interfaces. This differs slightly from the approach in [15], which includes as an input the boundary forces due to the next component, and finds the proper "control loop" such that the boundaries are constrained together.

Once the redundant coordinates are removing using a second state transformation $p = Sq$, the end result is the state-space representation of the assembled system,

$$\begin{Bmatrix} \dot{q}_r \\ \ddot{q}_r \end{Bmatrix} = \begin{bmatrix} 0 & I \\ -M_s^{-1}K_s & -M_s^{-1}C_s \end{bmatrix} \begin{Bmatrix} q_r \\ \dot{q}_r \end{Bmatrix} + \begin{bmatrix} 0 \\ S^T \begin{bmatrix} \Psi_A^T \beta_A \\ \Psi_B^T \beta_B \end{bmatrix} \end{bmatrix} \cdot F$$

$$\begin{Bmatrix} y_A \\ y_B \end{Bmatrix} = \begin{bmatrix} \begin{bmatrix} C_{yA}\Psi_A & 0 \\ 0 & C_{yB}\Psi_B \end{bmatrix} & 0 \end{bmatrix} \begin{Bmatrix} q_r \\ \dot{q}_r \end{Bmatrix}$$

The system can also be written in transfer function form. If the input is on component A, and the output on component B, then β_A has a value of 1 at the degree of freedom of the input and zeros elsewhere, and C_{yB} has a 1 at the degree of freedom of the output, and zeros elsewhere. β_B and C_{yA} are all zero, in this case. The transfer function is:

$$G_{AB}(s) = \frac{Y_B(s)}{F(s)} = \begin{bmatrix} 0 & C_{yB} \end{bmatrix} \cdot \Psi_B \cdot S \cdot [s^2 M_s + sC_s + K_s]^{-1} \cdot S^T \cdot \Psi_A^T \cdot \begin{bmatrix} \beta_A \\ 0 \end{bmatrix}$$

The inverse transfer function, with input on B and output on A is:

$$G_{BA}(s) = \frac{Y_A(s)}{F(s)} = \begin{bmatrix} 0 & C_{yA} \end{bmatrix} \cdot \Psi_A \cdot S \cdot [s^2 M_s + sC_s + K_s]^{-1} \cdot S^T \cdot \Psi_B^T \cdot \begin{bmatrix} \beta_B \\ 0 \end{bmatrix}$$

And since $C_{yA} = \beta_A^T$, and $C_{yB} = \beta_B^T$, these transfer functions are also the transposes of each other. The transfer functions should be the same, although some variations due to removed normal modes are likely.

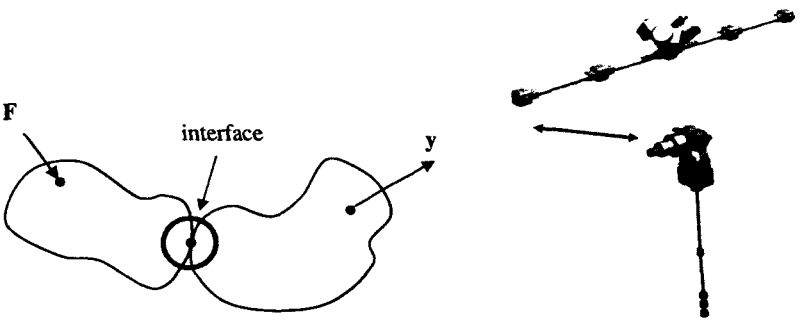

(a) Joining of generic components (b) Interface of MACE

Figure 9: Component interfaces

2.2.3 Interface Uncertainties

Next the modeling uncertainties at an interface of two generic structures are considered. On a more specific level, one could imagine the main boom of MACE being modeled separate from the gimbal and flexible appendage. The model would be assembled (using the Component Mode Synthesis approach proposed, for example) with the interface at the node-gimbal attachment degrees of freedom.

Along with all of the typical uncertainties in the models themselves (parametric, model error, etc.) uncertainties in the global system could also result from the assembly process and the interface itself.

The first source of interface uncertainties could be from the component mode synthesis method. One of the advantages of the method is that it reduces the number of states of the component models by keeping only a small subset of the normal modes. The final assembled model can then be constructed with only the critical states of each component retained. Although this reduction capability is an asset in working with large models, it has the potential to allow important dynamics to be lost in the reduction. Maghami and Lim [17] suggest that component modes up to twice the desired system bandwidth should be kept, but admit that even this will not guarantee accuracy in all cases. The uncertainty resulting from these eliminated modes must be considered. The easiest solution would be to run convergence tests, with different numbers of kept modes. Once the results begin to diverge, the acceptable limit of mode reduction has been reached.

A similar procedure could also be used to determine the effect of the choosing the wrong modes. The Craig-Bampton method uses normal modes with fixed boundaries and constraint modes, but there are other options. Normal modes can be found with fixed, free, or intermediate boundaries. Free body modes must be accounted for in the case of free body motion. Reference [7] describes some of these other options.

Another source of uncertainty could be model errors in the interface itself. Although the illustration in figure 9(a) shows the interface as merely a single point, physical inter-

faces could have static and dynamic behaviors of their own. For example an optics on a telescope may be separated from the noisy ground by an isolator assembly with its own dynamics. Thus, depending on the complexity of the interface, some or all of the standard model uncertainties might need to be included, including parametric and non-parametric uncertainties.

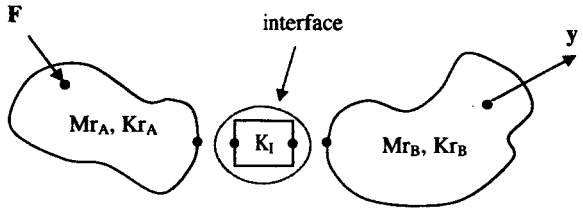

Figure 10: Component interface

A simple model of an interface would include only stiffness terms, and no dynamics. The standard illustration could be redrawn to show this (figure 10). The interface would become a part of the assembled system using

$$M = \begin{bmatrix} M_{rA} & & \\ & 0 & \\ & & M_{rB} \end{bmatrix} \qquad K = \begin{bmatrix} K_{rA} & & \\ & K_I & \\ & & M_{rB} \end{bmatrix}$$

Given Interior and Boundary states $[\ x_i^I \quad x_i^B\ ]^T$ for each component, the components can be assembled using the transformation

$$\begin{Bmatrix} x_A^I \\ x_A^B \\ x_I \\ x_B^I \\ x_B^B \end{Bmatrix} = \begin{bmatrix} I & 0 & 0 \\ 0 & I & 0 \\ 0 & I & 0 \\ 0 & I & 0 \\ 0 & 0 & I \end{bmatrix} \begin{Bmatrix} x_A^I \\ x_I \\ x_B^B \end{Bmatrix}$$

The interface stiffness uncertainty could then be described as $K_I = K + \Delta K$ for use in uncertainty calculations.

2.2.4 System Performance Uncertainty

Consider two alternate models for the assembled system. The first is a networked model in which all of the component models are fully retained as distinct entities.

This is akin to the integrated modeling approach, where complete, distinct models are combined together to form the total system response. Since the full system model for each component remains, all of the parametric uncertainties of the individual models can be retained and used to find the total system performance uncertainty. Both of the approaches described above are utilized in this case. The models are combined using Component Mode Synthesis. In addition to the uncertainties in the models themselves, interface uncertainties

can also be included. The combined model in state-space form gives the system performance using the Lyapunov disturbance to performance algorithm.

Given a collection of probabilistic uncertain parameters, the Latin Hypercube Sampling technique described initially can be used to examine the uncertainty space much faster than traditional Monte Carlo sampling. More parameters can be investigated than would be possible with the Change-of-Variables routine. One could also consider using First or Second Order Reliability Methods [18] (FORM/SORM).

The other approach to take is to build an aggregate model of the system which does not retain the individual physical parameters of the component models. This "tree" method of modeling, would usually result from models being built by different divisions or organizations. The separate models are then independently reduced from the full physical coordinates (thousands to hundred of thousands of degrees of freedom, perhaps) to a reduced set of non-physical coordinates. This reduction could use component mode synthesis, although other techniques such as Guyan reduction are also possible. In any effect, the reduced models are assembled into a global systems model elsewhere (up the "branches" of the tree-like organization, say) without reusing any of the lower-level component models. It is common in this case that reduced mass and stiffness matrices (M_{rA} and K_{rB}, using the notation above) are passed to the assembly process.

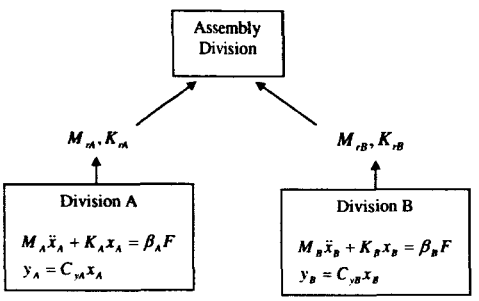

Figure 11: Tree model

In order to compute the total system uncertainty, the individual uncertainties in the components must still be passed along with the mass and stiffness models. It is therefore required that the parties responsible for the component models also prepare an uncertainty model.

One of the challenges in this case is that the physical coordinates are no longer available for the aggregate model. Therefore, the physical uncertainties used previously cannot be passed along. The challenge is to frame the uncertainties in the transformed coordinates, and pass these along as ΔM_{rA}, ΔK_{rA} terms. As shown in [11], it is relatively easy to use transformed, modal uncertainties such as modal mass, frequency, and damping, as uncertain parameters. In terms of component mode synthesis, [15] and [17] both choose to use only normal modes for the component mode basis. In this case, the reduced systems are in the familiar form

$$\begin{bmatrix} \ddots & & \\ & m_{ri} & \\ & & \ddots \end{bmatrix} \ddot{q}_i + \begin{bmatrix} \ddots & & \\ & 2\zeta_i\omega_{ri} & \\ & & \ddots \end{bmatrix} \dot{q}_i + \begin{bmatrix} \ddots & & \\ & \omega_{ri}^2 & \\ & & \ddots \end{bmatrix} q_i = \Phi^T \beta_i F$$

where m_{ri} is the modal mass, ζ_i is the damping, and ω_i is the natural frequency for component i. Using the transfer function from the component input to either the component output or the interface, the largest modal contributors to the cumulative RMS should be identified by the component organization, and singled out for inclusion in the component model.

In order to consider probabilistic uncertainty, it would be necessary also for the component organization to include information on the probability density of the uncertain modal parameters. This could be considered in two ways. Given that the component organization has access to all of the uncertain physical parameters, a probabilistic propagation routine could be used to directly compute distributions for critical modal parameters. These distributions could be passed along with the models. If there are a large number of uncertain parameters passed along however, it could be reasonable to invoke the central limit theorem, and assume that the modal parameters would tend toward a normal (Gaussian) distribution. Only the mean value for each modal parameter, along with a variance estimate would have to passed along in this case.

The model handed up the tree to the system assembly division would be of the form

$$M_{ri} = \bar{M}_{ri} + \Delta M_{ri} \qquad K_{ri} = \bar{K}_{ri} + \Delta K_{ri}$$

for component i, where the $\bar{M}_{ri}$ and $\bar{K}_{ri}$ are mean values, and the distribution is described in the Δ terms. As an example, if the frequency were normally distributed about a mean value contained in $\bar{K}_{ri}$, with standard deviation $\sigma_{\omega i}$, the uncertainty would look like:

$$\Delta K_{ri} = \begin{bmatrix} 0 & & \\ & \aleph(0, \sigma_{\omega i}) & \\ & & 0 \end{bmatrix}$$

The aggregate model can now be constructed without use of the lower level component models, still by using the assembly procedure described earlier for component mode synthesis. The performance can be computed using the same Lyapunov techniques described earlier. The same approach as before can be taken to compute the uncertain performance, namely by use of Latin Hypercube sampling over the uncertain parameter space. The key difference in this tree method is that the uncertain parameters are now in a transformed coordinate space which is much smaller than the original physical coordinate space.

2.2.5 Conclusion

Two methods of computing the performance uncertainty of a system comprised of two or more uncertain components was presented. The first method, the networked method, uses the entire component model and has at its discretion all of the uncertain physical inputs.

This is both an advantage and added difficulty. The advantage is that the global system modeler has a great amount of insight into the actual physical causes of system-level uncertainty. The design space has much greater fidelity since the effect of individual uncertainties can be identified. Resources can be brought to bear immediately on the physical sub-component responsible for the system uncertainty. Also, there is less approximation in this analysis technique, as compared with the tree method which must first approximate the uncertainty in terms of modal parameters.

These advantages of course are tempered by the great size of the full component models being used. Running the analysis will take more computer power. Also, there is the very real possibility of being overwhelmed by the sheer number of possible uncertain physical parameters. The critical effect of one component on another very well could be reduced to several important modal frequencies and a full physical system may not be necessary.

Model assembly using the tree method starts with the models reduced already. Uncertain modal parameters must be decided upon and included with the reduced models. The advantages here are that much smaller models are used in the uncertainty analysis, so that either less computer power is needed, or more probabilistic samples can be run. The system modeler also has a much simpler task of assigning uncertainty, since he/she is not responsible for the details of the component, but rather of only the critical effects. The disadvantage is of course loss of insight into causes of performance uncertainty. The system modeler can only isolate the component which creates the most uncertainty. Identification of the actual input causing the component to be uncertain can only be done by sending word back down the tree to the component group, which must investigate the problem and send back updated models. This process can take much longer than the networked method.

2.3 Role of MACE in Uncertainty Analysis

The MACE testbed is used extensively this research. It provides an excellent opportunity to examine uncertainty on an accelerated timeline, since the hardware is already designed, developed, and tested. Data are available in both 1-g and 0-g environments, across many years and with different sets of hardware. The presence of this testbed is a great advantage in uncertainty research, since any validation of uncertainty routines requires knowing the actual behavior of a modeled system. This access to working, tested hardware allows MACE to be "designed" anew, with immediate comparisons between those new designs and actual behavior. The design process can be recreated without the years of manufacturing normally required. In order to prevent knowledge already gained from MACE from influencing the uncertainty models of the new design, actual flight data will be kept separate until such time as would be appropriate in the design process.

The design process has been started anew on MACE. A new model has been constructed using Femap® (figure 12). It is based solely on original drawings of the MACE article, and uses handbook values for all materials. This model is akin to a preliminary "stick" model, often used to perform the very first dynamical analysis on a structure. There also exist MACE models of greater accuracy, whose parameters have been updated with data. While these models may be more accurate than this preliminary model, they also rely on data from hardware which may not exist in a real design process. These models together represent several stages of the the design process and are a valuable tool in testing

uncertainty approaches and in tracking uncertainty through a design. The updated MACE model is used in Section 5 to illustrate uncertainty analysis based on hardware testing.

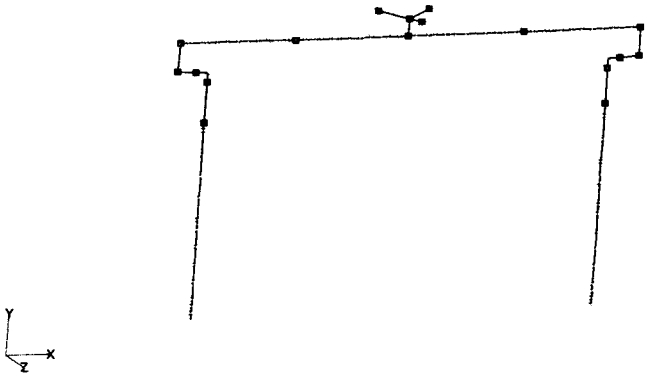

Figure 12: New finite element model of MACE

3 Uncertainty Source Investigation

The first step in placing uncertainty bars on the performance output is to identify those aspects of the model inputs that are most uncertain. Generally these may include both parametric uncertainties, representing all parameters explicitly contained in the model (e.g. Young's modulus or rotary inertias) and non-parametric uncertainties, defined as all other uncertainties that are not explicitly in the model (non-linear behavior, incorrect boundary conditions, etc.).

A list of many typical sources of model uncertainty in high performance optical systems was produced (table 1). It was made from a combination of literature on the subject and SSL experience dealing with uncertainty. The intention was to produce a comprehensive list which could be compared with a new design model; those items on the list which are present in the system can be given further consideration.

While this list identifies many *possible* sources of uncertainty, it is still necessary to identify those particular sources most likely to affect a particular design. A goal of uncertainty research should be to create a quantitative tool that can parse through such a comprehensive list and highlight sources for a model. Currently, engineering judgement is still necessary to decide which sources to investigate in greater detail.

Using MACE as an example, several uncertainty sources were chosen based on their expected influence on the model (all are expected to contribute to the final performance) and by the fact that all are relatively uncertain. These parameters are given in table 2, and consist both of parametric uncertainties such as modulus, and non-parametric uncertainties such as non-linear behavior in the strut-node connection.

One of the greatest difficulties with uncertainty modeling is that even when sources of

Table 1: Uncertainty Sources

Material	**Gravity**	**Environmental**
Modulus	Joint Pre-load (locking)	Temperature varying E
Density	Body forces	Temperature varying ν
Point mass	Pre-stiffening	Temperature varying d_{31}
Damping coefficient	Sag (coupling)	Preload (thermal strain)
Composite Ply Orientation	Gravity-sensor coupling	Moisture (mass, shape change)
Composite matrix chemistry	Suspension dynamics	Outgassing
	Pendulum modes	Air dissipation
Model Error	B/C compliance	Density variation of air
Mismodeled loading	B/C damping	Speed variation of light in air
Modeling simplication	B/C energy leakage	Acoustic noise
Rigid links	B/C noise sources	
Rigid substructures		**Non-Linear**
Beam approx. for truss	**Degradation**	Modulus non-linearity
Element formulation	Fastener hole wear	Bearing stiction
Boundary conditions	Change in modulus	Bearing rattle
Cross-inertias (bending, rotary)	Cracks/crack density	Bearing imbalance
Sensor misalignment	Bearing wear	Bearing shape irregularity
Rotation, translation		Joint stick/slip
Interface compliance		Loose fastener
Preload	**Manufacturing/Testing**	
(de)stiffening	Geometric tolerance	**Policy**
Static deformation	Material residual stress	Cost
Eccentric loading	Fastener Torque	
Joint rigidity	Preload	**Miscellaneous**
Gross incompetence		Optical effect of air

Table 2: Identified Sources of Uncertainty for MACE

Parameter	**NASTRAN card**
Young's modulus	`MAT1`
Rotational stiffness	`CELAS2`
I_{12} cross-bending inertia	`PBAR`
Non-linear interface	-

uncertainty are identified, very often there are no accurate models of how the source varies. This problem is particularly acute with probabilistic descriptions of uncertainty, as there are few references that give PDFs for common model inputs such as modulus. This lack of accurate uncertainty inputs casts a shadow on all of the analysis results, since without physically meaningful inputs the outputs are of dubious value.

Therefore, one of the goals of this work is to attempt to experimentally measure the distribution of prominent uncertainty sources. Two methods were used: direct testing of a MACE strut and model updating of selected NASTRAN input parameters.

3.1 Direct Measurement

If possible uncertainties are identified and the hardware exists, a model of the variation of the parameter or effect of the non-parametric error can be produced by empirical testing. This has been done with a node-strut-node component of MACE. The first source of uncertainty under investigation is the Young's modulus E of the polycarbonate making up the length of the strut. Modulus was used in the model updating routines performed with the MACE model and allowed very good fits of the model to the data. Despite this, it was not clear whether the updating routine pushed "too hard," and thus varied the value for this parameter outside of the physically realizable range. The other source of uncertainty investigated is possible non-linear behavior at the strut-node interface. Depending on the tightness of the the steel collar that holds the aluminum node to the polycarbonate strut (figure 13), it is expected that slip between the strut and node could manifest into non-linear behavior.

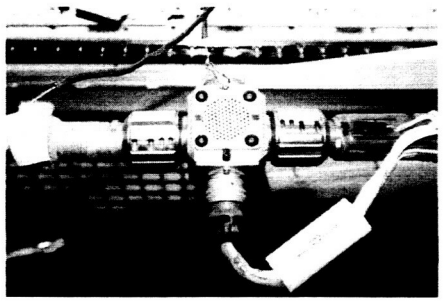

Figure 13: One of the MACE nodes, with two struts and collars connected

The first tests performed were axial compression tests using an Instron testing machine (figure 14). Since polycarbonate is an isotropic material, no difference in modulus was expected between bending tests and compression tests. The Instron machine applied increasing load at a rate of two pounds per minute. The load varied between -10 and -110 pounds. Load and displacement were measured by the testing machine, and strain was measured by a strain gage attached on the center of the strut. Example stress-strain and force-displacement plots are shown in figure 15. The stress was computed using the cross sectional area of the strut

$$\sigma = \frac{P_{measured}}{\pi(r_o^2 - r_i^2)} \tag{6}$$

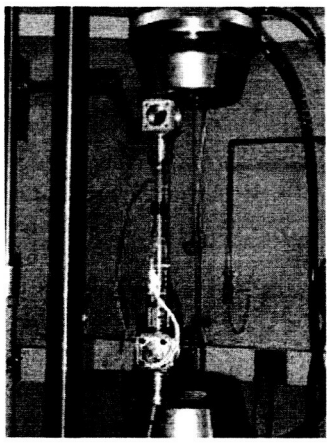

Figure 14: MACE strut compression test

where r_o is the outer radius of the strut, and r_i the inner radius.

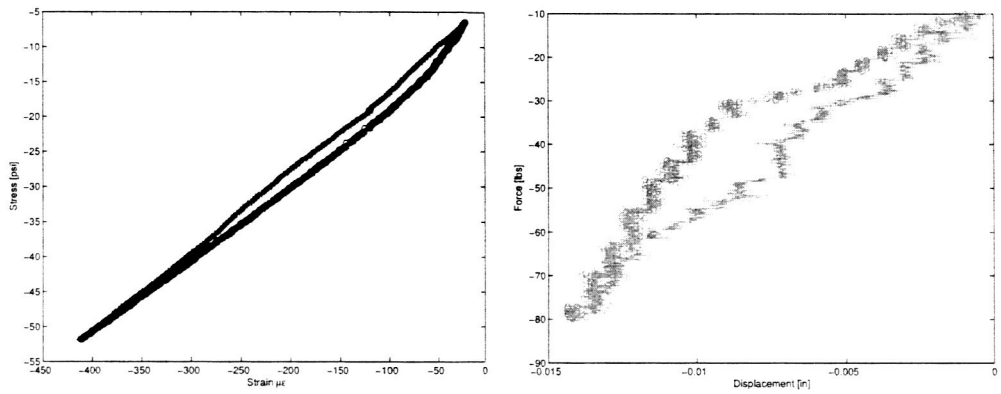

(a) Stress-Strain test

(b) Force-Displacement test

Figure 15: MACE strut compression test results

Upon inspection of the plots, it is obvious that the displacement data is much more noisy than the strain gage data, but trends can be seen in both. There is hysteresis which indicates non-linear behavior; this is not, however, considered to be the node-strut non-linearity expected. The interface slip should result when the load goes through zero; since only compression is being applied, that never occurs. In this case, the hysteresis in the force-displacement plot results from the strut being pushed axially into the node in compression. Since the strain gage measures strain just on the strut, the amount of hysteresis is much smaller than the displacement sensor which measures absolute displacement of the entire assembly. Because the load never goes through zero however, this test is only useful for measuring modulus.

By measuring the slopes of the resulting stress-strain curve, the averaged value for the

modulus was 117,000 psi. The data sheet for the particular material used (Zelux polycarbonate by the Westlake Plastics Company) lists a flexural modulus of 340,000 psi, nearly three times the value measured. This gross difference was extremely suspect, and was not taken as physically meaningful. Especially since the primary loads on MACE would be bending, rather than compression loads, it was decided that the test was incorrect for the entire component.

Following the failure of the compression tests, a bending test more akin to the expected loading on MACE was set up (figure 16). The strut was clamped to a laboratory bench. A L-beam was placed between the table and the fixed node in order to provide greater boundary condition rigidity. A point load was applied at the opposite node in order to produce bending. The load was applied by a stinger attached to a shaker. A loadcell was placed in the load path to measure resulting force.

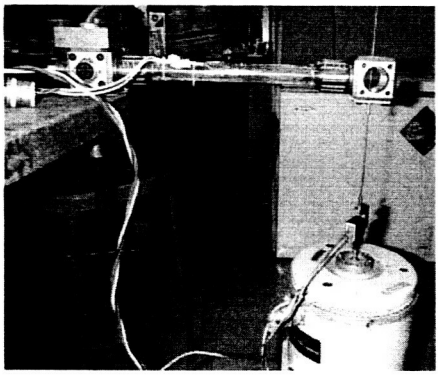

Figure 16: Strut bending test setup

The load was applied at 0.1 Hz and in such a manner that the displacement of the end node would go through zero. Bending strain was measured using strain gages at the center of the strut, and the stress is computed using Bernoulli-Euler beam theory with a point load.

$$\sigma_x(x) = -\frac{r_o}{I_{zz}} \left[-\delta_{stinger} + (L - x)\right] P_{loadcell} \tag{7}$$

r_o is the strut outer radius, I_{zz} is the area moment of inertia, L is the length, $P_{loadcell}$ is the force from the loadcell, and $\delta_{stinger}$ is a corrective term that takes the stiffness of the stinger into account.

The struts used are those of the MACE Engineering Model (EM), which was built for hardware testing before construction of the flight hardware. Three EM struts were available for testing, allowing difference between otherwise identical components to be examined. In order to determine the effect that collar tightness has on any non-linear behavior, the collars were turned to three levels of tightness, qualitatively defined as 'loose' (threads barely engaged), 'normal' (collar snug against the node), and 'tight' (as tight as possible by hand). Data was taken over multiple days, over a two month period.

An example stress strain curve is shown in figure 17. The most immediate observation is that the system is highly linear for all levels of collar tightness. Further, the collar tightness

seems to have no appreciable effect on the results. Even as the stress goes through zero (as the strut changes from bending downward to upward or vice-versa) there is no non-linearity detected. This is an important result, since it eliminates one of the potential sources of uncertainty. Now that non-linear behavior in the strut-node interface is shown not to be a factor, resources can be brought to bear examining uncertainties elsewhere.

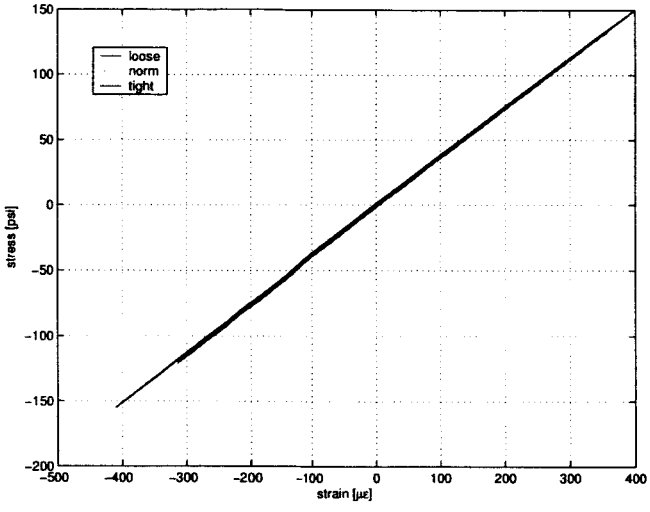

Figure 17: Stress-strain results from bending tests. EM strut #1, at three levels of collar tightness.

Modulus data is also taken from the slopes of the stress-strain curves. All data collected is shown in figure 18. Each strut is identified by a color. The collar tightness differences are again seen to be negligible. The modulus values are much closer to the published value, and taken as physically significant. The experimental moduli are all higher than the published value, between 375,000 psi to 403,000 psi. Figure 18 more significantly shows the differences between the three struts. The variation within a single strut is never more than 7,000 psi, while between struts can be upwards of 22,000 psi. This suggests that the subtle differences between otherwise identical hardware dominate the uncertainty. These differences may result from manufacturing tolerances or from the fit of the strut against the node. Likewise, a possible source of the difference could be sensor differences in the strain gages, and not a physical variation at all. This illustrates the difficulty in isolating the true source of component uncertainty.

The statistical mean and standard deviations of the individual strut data, along with the aggregate data, is given in table 3. The statistical significance of this can be questioned because of the very limited number of struts available. Whereas material coupon testing could use hundreds of samples to give confidence in the statistics of material modulus, tests of large components often have to make due with a limited number of hardware pieces. This restriction means that it would be difficult to produce detailed probability density functions with such samples. A much larger uncertainty effort, aimed at creating a true statistical database of material properties and other parametric model inputs would be highly advantageous to the field.

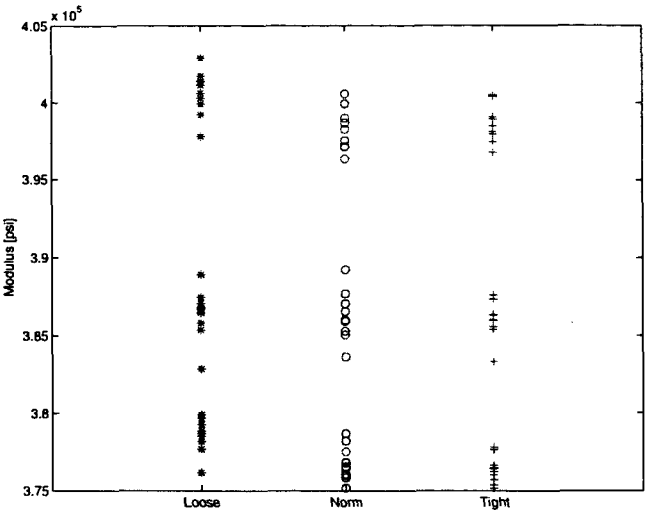

Figure 18: Averaged strut moduli for the three collar tightness levels. Colors represent strut #1 (blue), #2 (green), and #3 (red).

Table 3: Strut bending data statistics

	Mean	**Std. Deviation σ**
Strut #1	377,000 psi	1700 psi
Strut #2	386,000 psi	2500 psi
Strut #3	399,000 psi	1600 psi
Aggregate data	387,000 psi	9300 psi

Given the limited sample size with only the mean and standard deviations of the data, a Gaussian PDF is an acceptable distribution. Figure 19 shows the probability mass functions (PMF) of the discrete data points, overplotted by Gaussian PDFs.

The results of the component uncertainty tests show how difficult it can be to isolate and produce accurate distributions of identified uncertainties. However once uncertainties such as modulus or non-linearities are suspected, testing proves invaluable. The lack of non-linear behavior in the interface means that no more effort must be wasted in examining it. Even with the questions that remain on the statistics of the modulus data, the results show that the effective modulus is higher than the published values. A Gaussian PDF or 3σ bounds on the mean values still provides uncertainty information that would otherwise be complete guesswork.

Lessons learned include the need to create tests that properly capture the uncertainty under investigation. The MACE struts are loaded primarily in bending, so a bending test should have been performed first. For probabilistic analysis it is also necessary to have a large enough sample size to ensure statistical significance. For tests of larger components for which only a limited number of pieces are built, probabilistic analysis may be limited to Gaussian PDFs.

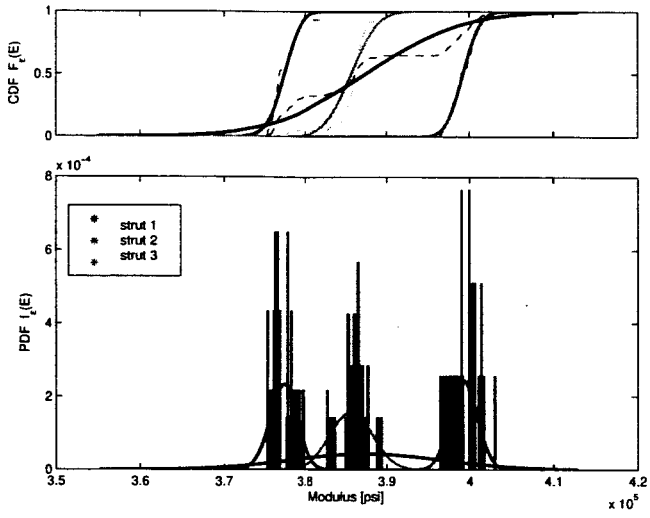

Figure 19: Gaussian PDFs from the bending test results with the individual struts in colors, and the aggregate data in black.

3.2 Physical Parameter Fitting

The second approach used to build uncertainty models is to use frequency response data to update model parameters via a tuning methodology. Using data from multiple test runs, a collection of parameter fits can be used to create a statistical model of those parameters.

The parameter tuning methodology in general is an iterative process, with a "coarse" stage in which large model changes are made to get the gross features of the model to match the measured response of the system. Then a "fine" stage is used to fine-tune the model. First, the tuning metric is chosen. Modal frequencies and Frequency Response Functions (FRFs) are good candidates for the coarse and fine stages, respectively, of the tuning process. Next, tuning parameters are chosen using engineering insight, and the functional dependence of the tuning cost on the parameters established. This stage is itself iterative, to find parameters that have the necessary effect on model response (modal frequencies and residues for example). Next the parameters are tuned to create a "best-fit" model, either manually or via nonlinear search methods. If the best-fit model is sufficiently accurate, the process is stopped. If not, the parameter set is not complete and additional tuning parameters are identified.

The parameter model is generated by creating multiple tuned parameter sets, once the complete set has been established.

The parameter model for the MACE MBP was created from physical parameter fits to three different data sets, taken on three different days after complete disassembly and reassembly of the MACE hardware. The parameters were chosen as those with the largest influence (highest sensitivity) in the FRF channels. The mean and standard deviation of the fits were computed using MATLAB standard functions, and independent Gaussian models were fitted to each parameter. The parameters are tabulated in table 4. The identified parameters and 3-sigma bounds are shown in figure 20. The parameters are:

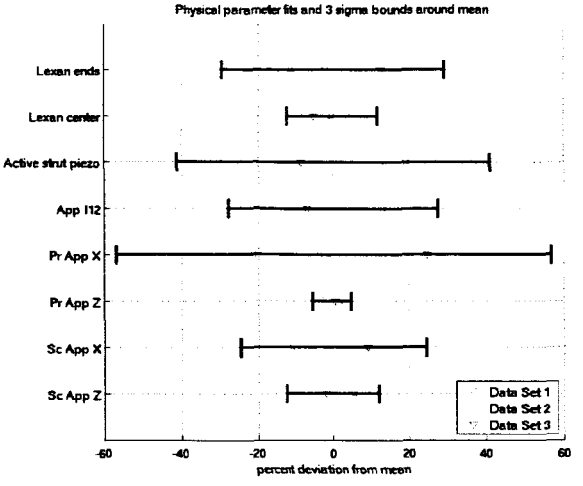

Figure 20: Physical parameter fits (plotted as deviations from mean of identified value) and 3-sigma bounds of Gaussian model.

Lexan end modulus, that models the node-to-Lexan strut interface; Lexan center modulus that models the struts themselves; the active strut piezo modulus; cross-inertia in the appendages that cross-couples bending motions; and Primary and Secondary Appendage base rotational stiffnesses that model compliance in the attachment between the appendages and the gimbals. Note in particular that the Primary Appendage base X stiffness has a very wide distribution. The variation in the fits was driven by the need to match a highly observable mode that changed by a few Hertz in frequency from test to test, and that was traced to a machining tolerance that left the appendage attachment screw slightly out of flush with the face of the gimbal. The result was a preload that was highly dependent on the tightness of the screw.

Table 4: Physical model update parameters

Name	**Description**	**Mean**	**Std. Dev.**
Lexan ends	Lexan/node attach point modulus	2.51 GPa	0.25 GPa
Lexan center	Lexan strut barrel modulus	2.77 GPa	0.11 GPa
Active strut piezo	Weighted piezo strut modulus	3.52 GPa	0.48 GPa
App. I_{12}	App. bending cross-inertia	53.4e-12 m^4	4.90e-12 m^4
Pr. App. X	Primary App base X rotational stiffness	444.3 Nm/rad	84.1 Nm/rad
Pr. App. Z	Primary App base Z rotational stiffness	762.0 Nm/rad	12.7 Nm/rad
Sc. App. X	Secondary App base X rotational stiffness	731.5 Nm/rad	59.9 Nm/rad
Sc. App. Z	Secondary App base Z rotational stiffness	832.2 Nm/rad	33.7 Nm/rad

4 Change-of-Variables Propagation Routine

The Change of Variables solution uses the Probability Density Function (PDF) transformation [5]

$$f_\Sigma(\sigma) = \left|\frac{\partial p}{\partial \sigma}\right| f_P(p) \tag{8}$$

to describe the PDF of the output σ to inputs p, given the PDF of the inputs, and assuming a relationship $\sigma = g(p)$. Generally this requires the functional relationship to be inverted $p = h(\sigma)$, so that

$$f_\Sigma(\sigma) = \left|\frac{\partial h(\sigma)}{\partial \sigma}\right| f_P[h(\sigma)] \tag{9}$$

For systems analysis, σ is often a performance found using frequency domain methods, with the inputs p buried in the process; in such situations is can be difficult to explicitly form the inverted relationship $p = h(\sigma)$ and the sensitivity $\partial p/\partial \sigma$. However, when the function is known implicitly, the form can still be used numerically to sample the PDF of σ . The approach is to rewrite the differential relationship as

$$\left|\frac{\partial \sigma}{\partial p}\right| \cdot f_\Sigma(\sigma) = f_P(p) \tag{10}$$

This is an algebraic relationship that can be solved for f_Σ:

$$f_\Sigma(\sigma) = \frac{f_P(p)}{\left|\frac{\partial \sigma}{\partial p}\right|} \tag{11}$$

which only requires the computation of the gradient of σ with respect to p. In the case of multiple input-multiple output systems, this becomes the determinant of the Jacobian J.

$$J = \det \begin{bmatrix} \frac{\partial \sigma_1}{\partial p_1} & \cdots & \frac{\partial \sigma_1}{\partial p_n} \\ \vdots & & \\ \frac{\partial \sigma_n}{\partial p_1} & & \frac{\partial \sigma_n}{\partial p_n} \end{bmatrix} \tag{12}$$

Note that an equal number of inputs and outputs are required so that the Jacobian remains square. If there are smaller number of output, "dummy" outputs must be included at this stage, and can be integrated out of the results later.

This approach to an output distribution is often described in textbooks on the subject, but is not found in research literature. Examples most often include simple single input-single output functions that can be solved analytically, with pencil and paper. This research has taken this procedure and applied it to much larger problems that cannot be solved as easily. An important step is to sample the functions, instead of attempting to perform the inversion. Given a range of values about the inputs p, the output σ, the input PDF $f_P(p)$ and the determinant of the Jacobian J can be computed at each value. equation 11 is used to compute the output PDF at each point. Finally, the output PDF values are mapped from the input p-space to the output σ-space, where they must be binned into the appropriate output grid space. The exact procedure is described next, using inputs x and outputs y for a relationship $y = g(x)$.

1. Grid input x
2. Pick x_o
3. Compute $f_X(x_o)$
4. Compute $y_o = g(x_o)$
5. Compute $\left|\frac{dy_o}{dx_o}\right|$
6. Compute $f_Y(y_o) = f_X(x_o) \cdot \frac{1}{\left|\frac{dy_o}{dx_o}\right|}$
7. Repeat steps 2-6 through the x-grid
8. Grid output y
9. Find all y_i in each Δy bin
10. Sum together all $f_Y(y_i)$ that correspond to those y_i in the bin for the final output distribution

4.1 Monotonic Example

This procedure will be demonstrated first with two simple examples. A full parameter-input to performance-output dynamic analysis will be shown in Section 5. First consider a system of equations described below, in which the inputs and outputs are related monotonically, i.e. through the sample space the gradients are never zero.

$$\begin{aligned} y_1 &= x_1 - x_2 \\ y_2 &= 4x_1 + x_1 x_2 \end{aligned} \tag{13}$$

This procedure makes no assumption on the distributions of the input parameters. For these examples, the Gaussian distribution is used to model the input PDFs.

$$f_{X_i}(x_i) = \frac{1}{\sqrt{2\pi\sigma_{x_i}^2}} \cdot \exp\left(\frac{-(x_i - \mu_{x_i})^2}{2\sigma_{x_i}^2}\right) \tag{14}$$

If the inputs are independent, their joint PDF can be formed by multiplication. The resulting distribution is plotted in figure 21.

$$f_{X_1,X_2}(x_1, x_2) = f_{X_1}(x_1) \cdot f_{X_2}(x_2) \tag{15}$$

The gradients can be found using the sensitivity functions of the DOCS toolsuite. For this simple example, the determinant of the gradient is quickly calculated analytically.

$$J_{ana} = x_1 + x_2 + 4 \tag{16}$$

And finally the output distributions in the x-space are computed via

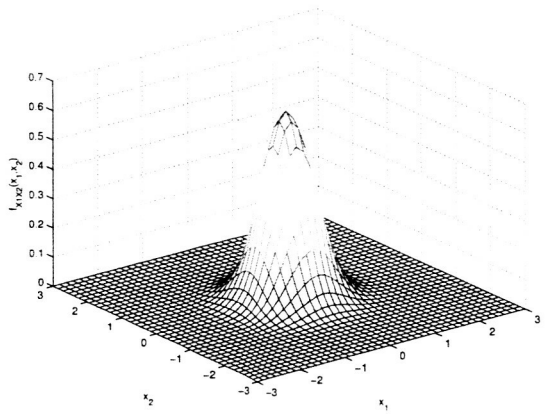

Figure 21: Joint PDF for two Gaussian inputs

$$f_{Y_1^x,Y_2^x}(y_1, y_2) = \frac{f_{X_1,X_2}(x_1, x_2)}{|J|} \tag{17}$$

This output PDF is shown in figure 22(a). Once the PDF values are mapped from the input-space to the output y-space, the PDF looks like figure 22(b). This surface is the joint PDF for both outputs. In order to solve for the individual PDFs f_{Y_1} and f_{Y_2} (if, for example, y_2 was a "dummy" output), the undesired output can be integrated out.

$$f_{Y_1}(y_1) = \int_{-\infty}^{\infty} f_{Y_1,Y_2}(y_1, y_2)\ dy_2 \tag{18}$$

This procedure can be done using numerically integration. The resulting individual PDFs and associated cumulative distribution functions (CDF) are shown in figure 23. Both CDFs asymptote to 1.0, guaranteeing that the output distributions are legitimate PDFs.

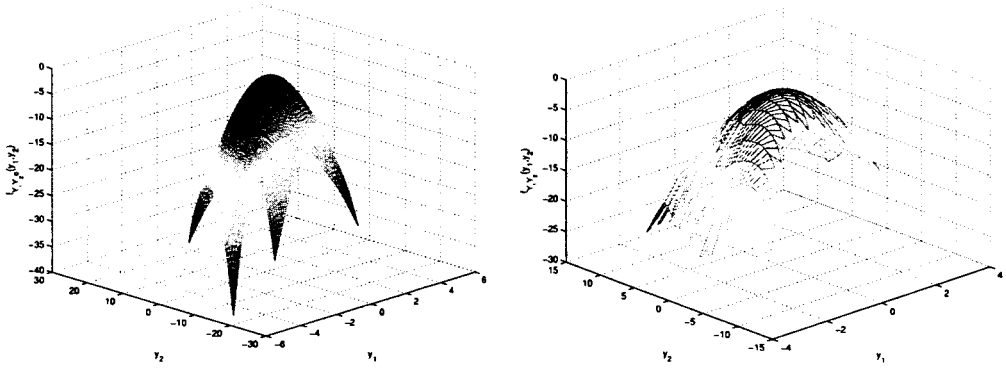

(a) Output PDF, whose points are mapped to the input grid

(b) Output PDF, whose points are mapped to the output grid

Figure 22: Output PDF mapping

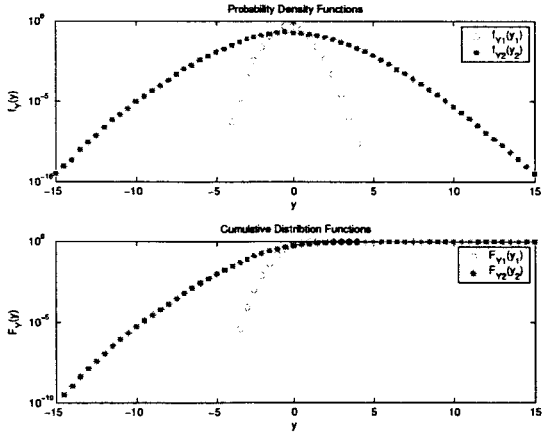

Figure 23: Output probability density functions (PDF) and cumulative distribution functions (CDF) for the monotonic example.

4.2 Non-Monotonic Example

The second example is of a similarly simples set of equations, but in this case the equations are non-monotonic. This results in gradients that go to zero. This will cause difficulties in equation 11, with J in the denominator.

The example system of equations is

$$\begin{aligned} y_1 &= x_1^2 + x_2^2 \\ y_2 &= 2x_1 + x_1 x_2 \end{aligned} \tag{19}$$

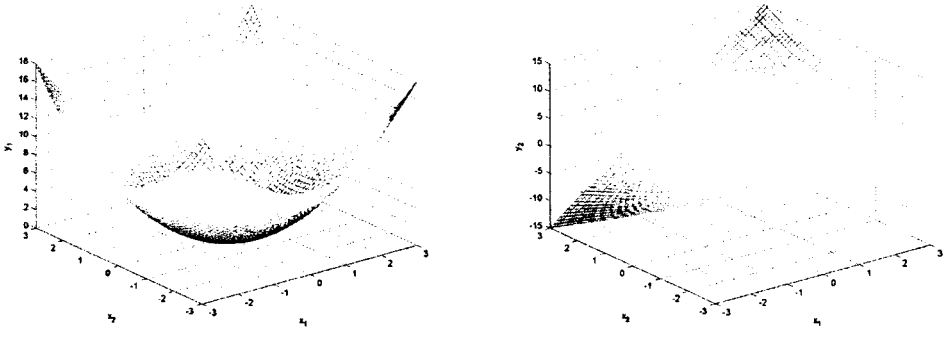

(a) Function $y_1(x_1, x_2)$ (b) Function $y_2(x_1, x_2)$

Figure 24: Example system of equations.

plotted in figure24, with analytical J as below. A plot of J is provided in figure 25.

$$J = 2x_1^2 - 4x_2 - 2x_2^2 \tag{20}$$

The difficulty is that the surface J (multi-dimensional if there are more than 2 inputs/outputs) goes through zero. As the steps are performed to compute the output PDF, a line of singularities appears. This can be seen as the PDF is plotted against the x points in figure 26(a), and again against the y points in figure 26(b). At this line the output PDF "wraps" around itself, creating two surfaces which must be summed together for the final output. It is also necessary to create a much finer mesh around the singularities, in order to capture the complete PDF; a coarse mesh will produce much higher values than actually exist. The Change-of-Variables code built allows for variable meshing, and provides the binning capability for non-monotonic systems such as this. The final resulting PDF for this example is shown in figure 27. An example using the MACE hardware is shown next.

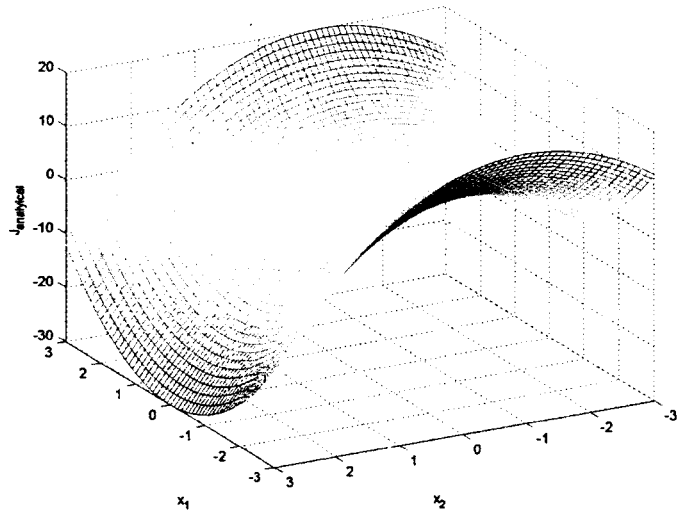

Figure 25: Determinant of the Jacobian. Note that in the non-monotonic example, a line of the surface passes through zero.

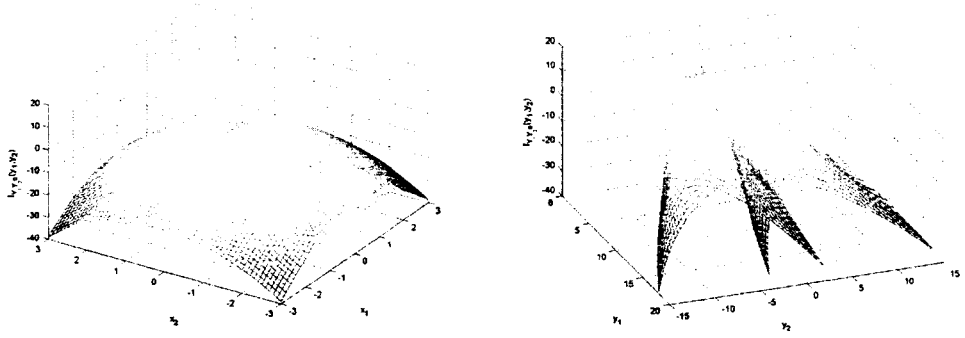

(a) Output PDF gridded in x-space

(b) Output PDF gridded in y-space, before binning. Note that the surface from plot (a) is wrapped about itself in this grid system.

Figure 26: Output PDF samples

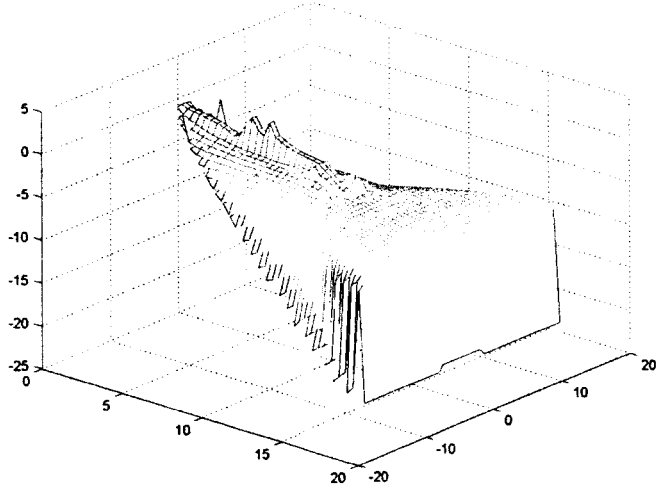

Figure 27: Resulting output PDF from `CoV_2D.m`.

5 Application of Uncertainty Analysis in the Design Process

All of the tools outlined in this report: legacy propagation tools, measured uncertainty parameter distributions, and the change-of-variables propagation routine, were used to illustrate an uncertainty analysis methodology with the MACE hardware. An overview of the framework developed in shown in figure 28.

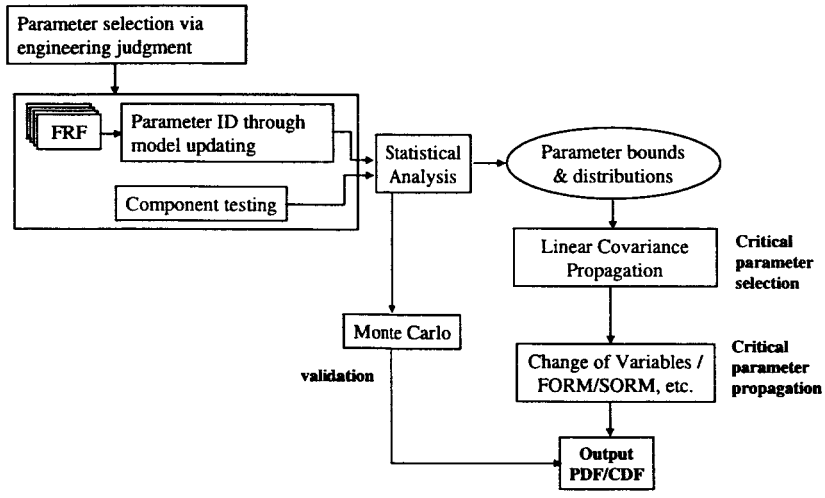

Figure 28: Uncertainty analysis framework. Data gained from component testing or hardware FRFs are used to generate a statistical model of dynamic model parameters. Resulting parameter sets are statistically analyzed to generate a parameter model. Linear Covariance Propagation is used to find the largest contributors to the performance variance, and Change of Variables analysis is used to determine the exact output PDF and CDF. Results are checked using Monte Carlo simulation.

The uncertainty analysis procedure used in this example is:

1. Conduct multiple experiments under varying test conditions (time, temperature, disassembly/assembly) to create multiple datasets of nominally identical hardware.

2. Perform a physical parameter identification on each dataset, in which parameters of the physical model are tuned to best fit the data. Create a statistical model of the identified parameters (by choosing the form of the distribution, and coefficients).

3. Perform an uncertainty contribution analysis using Linear Covariance Propagation (LCP) to identify the parameters that create the largest variance of the system design objective function.

4. Perform a Change-of-Variables (CoV) analysis on the parameters with the largest contributions to determine the exact design metric distribution.

5.1 Test System

The design approach is evaluated on the MACE Multibody Platform (MBP) in zero-gravity. Parameter studies and model updating were performed as part of the MACE Reflight, and provide the parameter database. This is a useful sample problem because it exhibits many of the features important in high performance controlled structures:

- coupled structural and control system dynamics, via sensor and actuator dynamics, and computer time delays
- closed loop control of the servoed gimbals and reaction wheel actuators
- high bandwidth flexible mode observability in the performance
- realistic scaling issues in the form of a wide frequency band (less than 1 Hz to over 100 Hz) and modal observability (Hankel singular values ranging from 495.8 to 8.9e-10)

The problem demonstrates propagation of physical uncertainties through a balanced state reduction and transformation to real-modal form. Additionally, the system will eventually support closed loop high bandwidth control studies.

The parameter model is that described in Section 3.2. The physical model parameters chosen by engineering insight, and updated using model tuning, are modulus of the lexan center and ends, modulus of the active strut piezo, appendage bending cross-interia, and rotational stiffnesses of the appendages. Table 4 gives the mean and standard deviations for all of the parameters.

5.2 Objective Function

The design objective for the MACE mission is to hold the 2-axis inertial pointing angle of the Primary Appendage (PrApp) under 2-axis white noise commanded slewing of the Secondary Appendage (ScApp). This is posed as the Root Sum Squared (RSS) PrApp pointing error as measured by the Primary Rate Gyro X (PRX) and Primary Rate Gyro Z (PRZ) sensors, which is a scalar cost:

$$J = \sqrt{E[PRX^2] + E[PRZ^2]} \tag{21}$$

The scalar RMS of PRX and PRZ will also be examined to understand the relative importance in the cost.

The units of the design model are nanometers to degrees. For the purposes of evaluating probability of success, the RSS requirement is set to be 5% larger than the predicted RSS (in other words, that the system achieves the requirement with a margin of 5%).

A unit torque intensity is assumed, which is within the capability of the actuators. In order to avoid exciting the low-frequency dynamics (due to the tethers which "stationkeep" the MBP inside the Middeck), the disturbance actuators are shaped with a filter that removes low (below 5 Hz) and high (above 200 Hz) frequency disturbances (figure 29). This has the effect of making the flexible mode dynamics more important in the pointing RMS. Without the filter, low-frequency components in the disturbance cause excessive pointing

errors due to rigid body motion, which wash out any flexible dynamics which are functions of the structural parameter uncertainties.

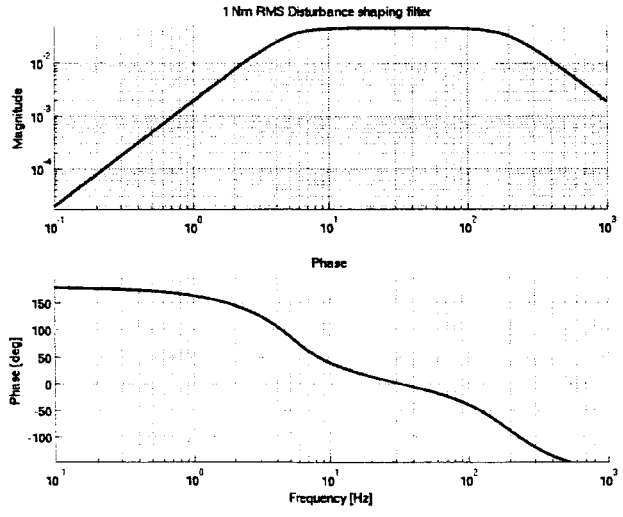

Figure 29: Disturbance shaping filter used to de-emphasize low frequency modes.

5.3 LCP Results

The first step is to evaluate the combined effect of all uncertainties in the quick but approximate LCP analysis.

The CDF and PDF of the RSS pointing error, computed using LCP, is plotted in figure 30 (top and bottom respectively). The horizontal red line in the top plot shows the probability of meeting the requirement of 5.99 deg (vertical red line) which is 79% in this case. The vertical red line shows the mean output RSS pointing error of 5.70 degrees, with variance of 0.35 degrees (6.1% variance).

The mean and variance of the RMS pointing error of each axis is computed using LCP. The PDF and CDF of the RMS of PRX is plotted in figure 31(a), and of PRZ in figure 31(b). The PRX axis is both the largest contributor to the RSS (contributing 4.91 as compared to 2.91 deg) as well as to the variance. This relationship is made even more clear in the following analysis.

A useful way to determine the relative importance of uncertain parameters is to look at the contribution of each to the total variance. This quantity is plotted for the RMS X and Z motions in figure 32. The top plot shows the mean value and 3-sigma bounds of each component of the RSS on the Y axis, for each component plotted on the X axis. The PRX RMS motion is clearly the dominant source. The bottom plot shows the normalized contributions of each uncertain parameter variance (color coded by the legend) to each component of the RSS. This result shows that the uncertainty in the PRX RMS variance is due primarily to variance in the Primary Appendage X-axis rotational stiffness. Since the PRX RMS is the largest contributor to the RSS, the same parameter dominates the

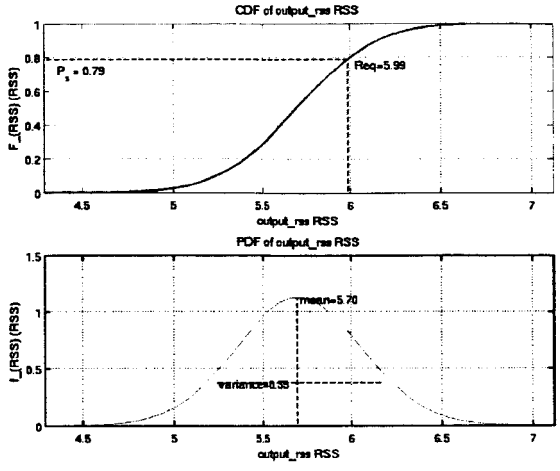

Figure 30: RSS pointing error computed using LCP. Top, CDF, bottom PDF. Red lines assume nominal design achieves a margin of 5%.

uncertainty in the RSS as well. In the Z component, the active strut and Lexan center moduli are dominant contributors.

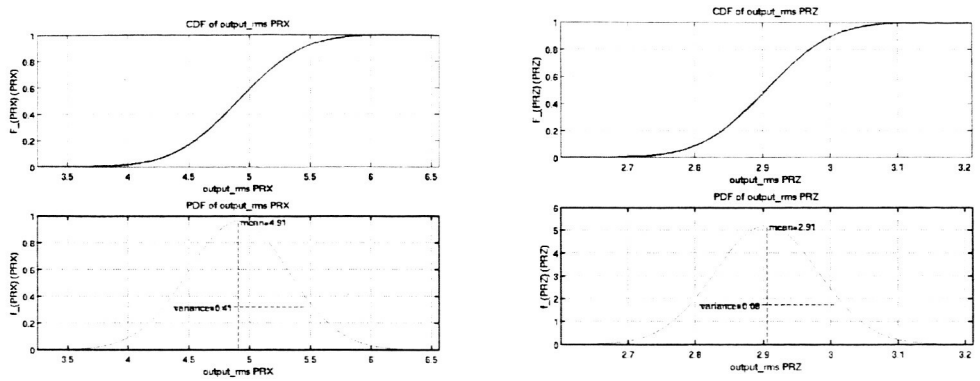

(a) PRX (b) PRZ

Figure 31: CDF and PDF of PRX and PRZ RMS computed using LCP.

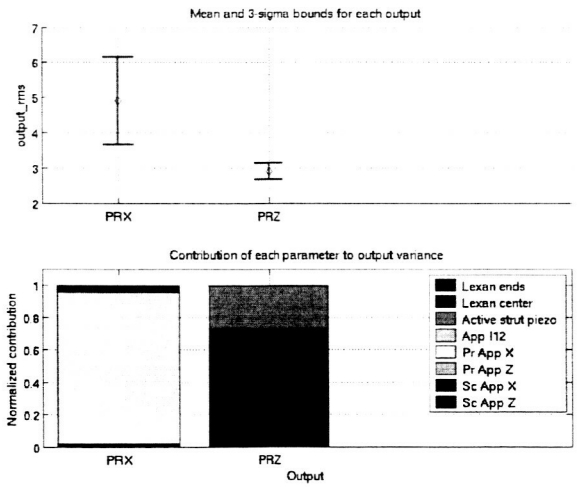

Figure 32: Contributions of each parameter to output RMS.

5.4 Change of Variables Results

The output RSS is next examined using the exact transformation from the distributions of Lexan end and center moduli, and the Primary Appendage X rotational stiffness. The resulting CDF and PDF of J is plotted in figure 33. The red line is the exact PDF computed using CoV. The green line is the LCP solution. The blue bars are the Monte Carlo check computed using 2000 samples with Gaussian distribution. The CoV result shows that the true distribution of the RSS "tails" very slightly off to the right (high RSS) side. This results in a slightly decreased probability of success (74% versus 79%). This would, however, potentially create more difficulty in achieving a higher probability of success (above 99%) since the mean might need to be lowered significantly. Alternatively, lowering the sensitivity of the RSS to the uncertainty in the Primary Appendage Base X stiffness would reduce the variance of the RSS and should be "cheaper".

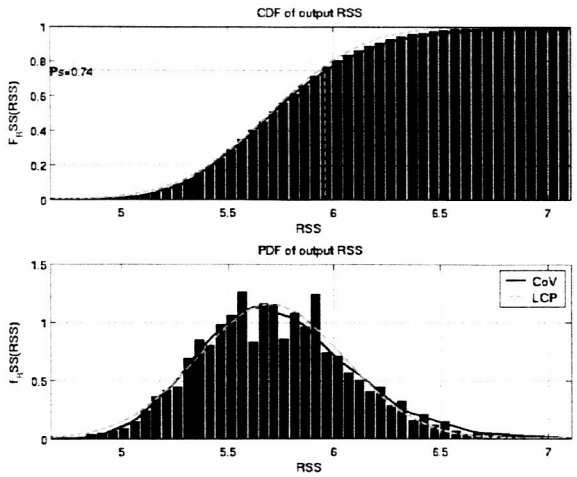

Figure 33: Comparison of CoV (red), LCP (green), and Monte Carlo (blue bars) for 3 significant parameters.

As a final check, a Monte Carlo analysis under uncertainty in all 8 parameters is performed, and compared to the CoV solution (figure 34). The Monte Carlo results do not show any dramatic differences compared to the CoV solution, verifying that the identified critical parameters are, in fact, the primary contributors to variance of the metric.

The relative computation times of the LCP, CoV, and Monte Carlo methods are of interest. The computation times for the 3-parameter solution are given in table 5. The LCP solution is the quickest method, and also provides useful information about the relative importance of different parameters. However, it cannot accommodate nonlinear and/or non-monotonic cost functions, or non-Gaussian parameter distributions. The Change of Variables procedure takes substantial computational effort (not only to compute but also to regularize, or map onto a uniform grid, the samples). However, it gives the exact shape of the PDF/CDF for nonlinear/non-monotonic functions and arbitrary input distributions, and is efficient to compute the tails of the distribution. The Monte Carlo solution time

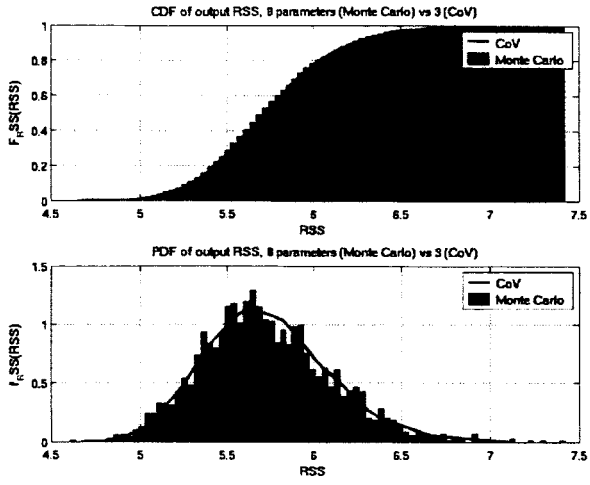

Figure 34: Comparison of CoV solution for 3 significant parameters (red) with Monte Carlo for all 8 parameters (blue bars).

will increase moderately as the number of parameters increases. However, the number of computations needed to accurately map the tails may be problematic.

Table 5: Relative computation times

3 Parameter Solution	**Solution Points**	**Time [sec]**
Linear Covariance Propagation	1	2.76 sec
Change of Variables	1000	285.2 sec
		(+1331.4 sec to regularize)
Monte Carlo	2000	467 sec

5.5 Deliverables

The Uncertainty Toolbox contains several uncertainty propagation tools, plotting functions, and analysis functions. A Command Reference Manual (DOCS_Uncertainty_Reference) is also posted at the DOCS Web server.

5.6 MACE Example Conclusions

- Uncertainty analysis was performed for a realistic sized problem given:
  - a flight vehicle with flexible structural dynamics
  - integrated structural/electronic dynamics
  - closed loop (servo controlled gimbals and reaction wheels)

Table 6: MATLAB Deliverables

	Function	Description
propagation	`CoV_1D`	1-parameter Change of Variables
	`CoV_2D`	2-parameter Change of Variables
	`CoV_3D`	3-parameter Change of Variables
	`lcp`	Linear Covariance Propagation
	`montecarlo`	Monte Carlo simulation
analysis	`bin_montecarlo`	Create histogram
	`pdf_Ps`	Find Probability of Success from a 1D PDF
	`pdf_statistics`	Find mean/variance from 1D PDF
plot	`plot_pdf`	Plot 1D PDF
	`plot_gaussian`	Plot a Gaussian distribution
	`plot_gaussian_contributions`	Plot contribution of each parameter to total variance
	`plot_montecarlo`	Plot Monte Carlo histogram

- Large parameter variance (19%) results in only moderate objective variance (6.1%)
  - Large parameter variance was required to match FRF of model to data
  - Mode frequencies don't have large influence on RSS (energy is still there)
  - the cost is nearly linear
- Stability is a function of modal frequencies.
  - Should be more sensitive to critical parameters

5.7 Independence of Output PDF

The change-of-variables solution approach is powerful, but cannot be applied to practical systems for more than three parameters at a time. The question arises whether the dependence of the cost function to each parameter could be nearly independent. This would allow PDFs from separate, computationally tractable analyses to be combined. For independent random variables (x_1,x_2) the PDF of the joint distribution is the product of the individual distributions,

$$f_{x_1,x_2}(x_1, x_2) = f_{x_1}(x_1) \cdot f_{x_2}(x_2) \tag{22}$$

Unfortunately test cases showed that the coupling of parameters through a function invalidated the independence property.

6 Conclusion

The objective of this research was to develop design methods and tools to the aerospace vehicle design process which take into account lifecycle uncertainties. The MIT SSL met this objective by investigating approaches to uncertainty identification and propagation, by using component testing to provide quantitative uncertainty descriptions, and by testing an approach to uncertainty analysis on the MACE testbed.

MACE was used as a example of a flexible, high performance vehicle. New models of the structure have been built in order to recreate the "preliminary" design stage. This allows uncertainty analyses to be performed on an early-stage model, with the hardware available for analysis validation. A listing of potential uncertainty sources was provided, and engineering insight was used to select those sources most likely to affect the output performance.

The benefits of uncertainty testing became very apparent. Non-linearity in the strut-node interfaces was considered a very likely source of uncertainty before testing showed it was not present. Testing saved time and resources on attempting to model an uncertainty that wasn't there. Likewise, parametric testing for modulus, rotary inertias and stiffness provided data-based distributions in place of educated guesses.

The change-of-variables propagation routine was developed. Although only capable of propagating at most three inputs through the system, it provides greater detail at the tails of the output distributions than linear covariance propagation or Monte Carlo sampling could. The routines were coded into MATLAB and have expanded the capabilities of DOCS.

Lastly, all of these research directions were combined in an uncertainty analysis of MACE. Several propagation routines were used to identify critical uncertainty sources, and propagate these through the model. This showed that such uncertainty analyses are possible for realistically-sized problems.

7 Mapping Research to the SOW

	Statement of Work	Work Performed
1)	Use the DOCS toolset to conduct design optimizations to not only maximize performance but augment that design process (using MIT's sensitivity and uncertainty analyses) with an ability to also minimize sensitivity to design error or uncertainty (maximize performance while minimizing error bars).	The DOCS toolset was used in analyzing the MACE model, including model updating and the uncertainty analysis. The design process augmented with measured parametric input bounds, along with the Change-of-Variables MATLAB codes (new addition to DOCS) plus other supporting codes. Sensitivity to uncertainty is reduced by identifying and characterizing uncertain parameters, and through the MACE uncertainty analysis. Importance of testing shown by elimination of suspected uncertainties (strut-node non-linearity).
2)	Use Markov reliability analysis tools to develop a methodology for reliability optimization. If improvements in mean time to failure as a function of funds spent, and the cost of redundancy in design, can be modeled, optimal control techniques can be used to identify where funding can be most effectively spent in order to maximize lifecycle productivity in the presence of failures.	Method for reliability optimization developed and published in Wertzs Masters thesis [21].
3)	Apply these tools to two different Aerospace examples. In the first, fatigue life of aerodynamic surfaces will be used as an example for maximizing fatigue life while minimizing sensitivity to uncertainty. The second example will be interferometry where optical metrics will be optimized.	Tools applied to two different aerospace examples. Reliability applied to a distributed node network in Wertz's Masters thesis. In place of aerodynamic surfaces, the uncertainty analysis applied to the pointing error (akin to optical pointing metrics) of a flexible controls platform (MACE). Using MACE allowed direct testing of hardware which was a great benefit in examining the uncertainties between model and data.

References

[1] Christine M. Belcastro. Parametric uncertainty modeling: An overview. In *Proceedings of the American Control Conference*, Philadelpha, Pennslyvania, June 1998.

[2] M.A. Blair, J.W. Sills Jr., and A. Semple. Determination of the model uncertainty factor using cross-orthogonality and overall load factor decomposition. In *Proceedings of the 12^{th} International Modal Analysis Conference*, volume 1, pages 613–618, Honolulu, Hawaii, 1994. Society for Experimental Mechanics, Inc.

[3] Carl Blaurock and David W. Miller. *Modeling of Geometrically Nonlinear Flexible Structures for Control.* PhD thesis, Massachusetts Institute of Technology, Cambridge, MA, September 1997. SERC #7-97.

[4] Frédéric Bourgault and David W. Miller. Model uncertainty and performance analysis for precision controlled space structures. Master's thesis, Massachusetts Institute of Technology, Cambridge, Massachusetts, December 2000. SERC #5-00.

[5] R.G. Brown and P.Y.C. Hwang. *Introduction to Random Signals and Applied Kalman Filtering.* John Wiley & Sons, New York, 3rd edition, 1997.

[6] Mark E. Campbell. *Uncertainty Modeling for Structural Control Analysis and Synthesis.* PhD thesis, Massachusetts Institute of Technology, Space Systems Laboratory, January 1996. SERC #2-96.

[7] Roy R. Craig Jr. *Structural Dynamics: An Introduction to Computer Methods.* John Wiley & Sons, New York, 1981.

[8] Hadi Dowlatabadi, Milind Kandlikar, and Charles Linville. Climate change decision-making: Model & parameter uncertainties explored. In *International Society for Bayesian Analysis, Third World Meeting*, Oaxaca, Mexico, September $28 - 30^{th}$ 1995.

[9] Roger G. Ghanem and Pol D. Spanos. *Stochastic Finite Elements: A Spectral Approach.* Springer-Verlag, New York, 1991.

[10] Anthony A. Giunta, Steven F. Wojtkiewicz Jr., and Michael S. Eldred. Overview of modern design of experiments methods for computational simulations. In *41st Aerospace Sciences Meeting and Exhibit*, Reno, Nevada, January 6-9 2003. American Institute of Aeronautics and Astronautics. AIAA 2003-649.

[11] Homero L. Gutierrez and David W. Miller. *Performance Assessment and Enhancement of Precision Controlled Structures During Conceptual Design.* PhD thesis, Massachusetts Institute of Technology, Space Systems Laboratory, February 1999.

[12] T. Hasselman. Quantification of uncertainty in structural dynamic models. *Journal of Aerospace Engineering*, 14, 2001.

[13] Roy R. Craig Jr. and Mervyn C.C. Bampton. Coupling of substructures for dynamic analyses. *AIAA Journal*, 6(7):1313–1319, July 1968.

[14] R.R. Craig Jr. Methods of component model synthesis. *The Shock and Vibration Digest*, 9(11):3–10, 1977.

[15] Kyong B. Lim. Robust control design framework for substructure models. *Journal of Guidance, Control, and Dynamics*, 19(1):181–190, January-February 1996.

[16] N. Logothetis and H.P. Wynn. *Quality Through Design: Experimental Design, Off-line Quality Control, and Taguchi's Contributions.* Oxford Series on Advanced Manufacturing. Clarendon Press, Oxford, 1989.

[17] Peiman G. Maghami and Kyong B. Lim. Substructure synthesis: A controls approach. Technical Report AIAA-99-3957, American Institute of Aeronautics and Astronautics, 1999.

[18] R. E. Melchers. *Structural Reliability Analysis and Prediction.* John Wiley & Sons, New York, 1999.

[19] David W. Miller, Edward F. Crawley, Jonathan P. How, et al. The middeck active control experiments (MACE): Summary report. Technical Report SERC #7-96, Massachusetts Institute of Technology, Space Engineering Research Center, Cambridge, Massachusetts, June 1996.

[20] Douglas C. Montgomery. *Design and Analysis of Experiments.* John Wiley & Sons, New York, 5th edition, 2001.

[21] Julie Wertz. Reliability and productivity modeling for the optimization of separated spacecraft interferometers. Master's thesis, Massachusetts Institute of Technology, Cambridge, Massachusetts, May 2002. SERC #9-02.